



# Microplane damage model for fatigue of quasibrittle materials: Sub-critical crack growth, lifetime and residual strength



Kedar Kirane<sup>a</sup>, Zdeněk P. Bažant<sup>b,\*</sup>

<sup>a</sup> Department of Mechanical Engineering, Northwestern University, 2145 Sheridan Road, Evanston, IL 60208 USA

<sup>b</sup> Department of Civil and Environmental Engineering, Northwestern University, 2145 Sheridan Road, Evanston, IL 60208 USA

## ARTICLE INFO

### Article history:

Received 15 May 2014

Received in revised form 24 August 2014

Accepted 26 August 2014

Available online 16 September 2014

### Keywords:

Microplane model

Quasibrittle

Fatigue

Paris law

Size effect

## ABSTRACT

In contrast to metals and fine grained ceramics, fatigue in concrete and other quasibrittle materials occurs in a large fracture process zone that is not negligible compared to the structure size. This causes the fatigue to be combined with triaxial softening damage whose localization is governed by a finite material characteristic length. A realistic model applicable to both has apparently not yet been developed and is the goal of this paper. Microplane model M7, shown previously to capture well the nonlinear triaxial behavior of concrete under a great variety of loadings paths, is extended by incorporating a new law for hysteresis and fatigue degradation, which is formulated as a function of the length of the path of the inelastic volumetric strain in the strain space. The crack band model, whose band width represents a material characteristic length preventing spurious localization, is used to simulate propagation of the fatigue fracture process zone. Thus the fatigue crack with its wide and long process zone is simulated as a damage band of a finite width. For constant amplitude cycles, the model is shown to reproduce well, up to several thousands of cycles, the Paris law behavior with a high exponent previously identified for concrete and ceramics, but with a crack growth rate depending on the structure size. Good agreement with the crack growth histories and lifetimes previously measured on three-point bend beams of normal and high strength concretes is demonstrated. The calculated compliance evolution of the specimens also matches the previous experiments. The model can be applied to load cycles of varying amplitude, to residual strength under sudden overload and damage under nonproportional strain tensor variation. Application to size effect in fatigue is relegated to a follow-up paper, while a cycle-jump algorithm for extrapolation high-cycle fatigue with millions of cycles remains to be researched.

© 2014 Elsevier Ltd. All rights reserved.

## 1. Introduction and objective

Although extensive research results on the sub-critical fatigue crack growth in metals and ceramics have been accumulated they are not applicable to quasibrittle materials, for three reasons:

- (1) The modeling of fatigue is inseparable from the modeling of distributed triaxial softening damage, which is rather intricate for quasibrittle materials;
- (2) because of material heterogeneity, the size of the fracture process zone (FPZ) is not negligible compared to structural dimensions (see Fig. 1); and
- (3) the finiteness of FPZ size, representing the material characteristic length, engenders a structural size effect on the rate of fatigue fracture growth (the size effect will be addressed in a follow-up article).

The size effect on the Paris law for fatigue fracture growth has been demonstrated in two previous studies and described on the basis of equivalent linear elastic fracture mechanics (LEFM) [1,2]. But no general model for combined fatigue and nonlinear triaxial softening damage appears to exist. The purpose of this paper is to develop such a model. The microplane model M7, which is a new and most advanced model for damage in concrete, with the broadest experimental verification, is adopted as the starting point.

Quasibrittle materials are heterogenous materials with brittle constituents. They include concretes, as the archetypical case, fiber composites, tough ceramics, sea ice, rock, stiff soils, rigid foams, wood, coal, bone, various bio- and bio-inspired materials, etc. All brittle materials become quasibrittle on sufficiently small scale. Thus brittle materials in micrometer scale devices (MEMS) must be expected to exhibit quasibrittle fatigue behavior similar to the behavior of concrete on the scale of meters.

The crack growth in brittle materials follows the Paris law [3], which reads,

\* Corresponding author. Tel.: +1 847 491 4025; fax: +1 847 491 4011.

E-mail address: [z-bazant@northwestern.edu](mailto:z-bazant@northwestern.edu) (Z.P. Bažant).

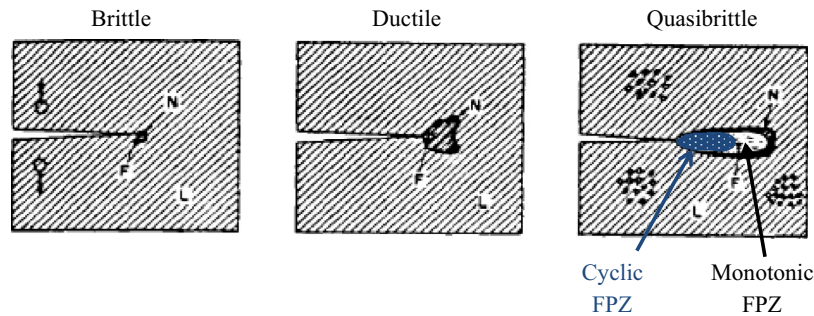


Fig. 1. Shape of nonlinear zone and fracture process zones [34] (L = linear zone, F = Fracture process zone, N = nonlinear zone).

$$\frac{da}{dN} = C(\Delta K)^m \quad (1)$$

where  $C$  and  $m$  are empirical constants depending on factors such as the environment, and load ratio [4]. The Paris law has been shown to apply also to concrete if the structure size is kept constant [1,2], and under this constraint it probably applies to all quasibrittle materials. The Paris law exponent  $m$  is typically between 2 and 4 for metals, while for concrete and ceramics it is about 10–50 [1,2,5,6]. Unlike metals, concrete exhibits a size effect on the crack growth rate [1,2], and so do rocks [7]. The microstructural fatigue mechanism, which is well known for metals [8,9], is not yet well understood for concrete but is sure to be quite different. Its understanding will be helped by the FPZ analysis which follows.

Fracture in concrete is characterized by distributed post-peak softening damage within a FPZ whose size is not negligible compared to structural dimensions [10]. The difference from embrittled metals is that the FPZ that travels forward with the fatigue crack growth is large. For metals, the FPZ is of micrometer size, and thus is negligible for specimens of centimeter size or larger. Therefore, interactions between triaxial damage and fatigue crack growth are insignificant. Not so, however, for quasi-brittle materials. The load cycles produce residual stresses in the cyclic FPZ, which is expected to be smaller than the monotonic FPZ but still large enough for such interactions. Under stable subcritical crack growth, the fatigue crack grows while interacting with progressive damage in the advancing FPZ. In the final stage, as the effective stress intensity factor of the equivalent LEFM crack increases, the crack advance accelerates and leads to stability loss, i.e., failure. The FPZ undergoing softening damage in concrete has been modeled by the cohesive crack model, in which the full FPZ width is lumped into an interface between two opposite crack faces and the softening damage is described by a traction-separation law [11–13]. In this approach, however, the tensorial behavior of the FPZ is not captured and the minimum possible spacing of parallel non-localizing cracks is not enforced.

To capture full tensorial behavior in the FPZ, including the effect of normal stresses parallel to the crack plane, one may use the crack band model (see [14], with implementation in [15] for a commercial code and arbitrary constitutive law). In this model, the inelastic softening damage is smeared within a crack band of a finite reference width that is a material property. The band width can be changed by adjusting the steepness of post-peak softening so as to maintain the same energy dissipation (although this is not what is done here, in order to minimize the approximation error associated with changing the crack band width). The reference band width serves as a material characteristic length representing a localization limiter, which prevents spurious mesh sensitivity of results [16]. For a very thin crack band, the cohesive crack model can be approximated closely. Another advantage of the crack band model is that it can simulate the width of the

FPZ, and consequently it can represent with correct spacing a system of parallel cracks when they do not localize, as in the presence of reinforcing bars or for some thermal stress distributions.

### 1.1. Previous studies of cohesive and constitutive models for fatigue

To predict the fatigue crack growth, the unload–reload hysteresis of the material must be captured realistically. Especially, the deformation increment over a cycle must be predicted correctly. The hysteresis was simulated by a number of researchers using the cohesive crack model.

In [17], the uniaxial cohesive stress–strain curve was adjusted downward after each cycle by an amount corresponding to the energy dissipated in the cycle. Another model [18] introduced a hysteretic cohesive law with different incremental stiffnesses depending on whether the cohesive surface opens or closes. This model was able to reproduce fatigue crack growth of Paris-law type and also some deviations from this law including short crack growth and the retarding effect of sudden overload in metals. In [19], an extension of this model with development of residual tensile stresses in the FPZ was shown to simulate fatigue crack growth under cyclic compression. In [20], a cohesive zone model with polynomial expressions for loading and unloading paths was proposed. Other similar approaches included the models by Horii [21], Bahn and Su [22], Bažant and Planas [10] and the continuous function model by Hordjik and Reinhardt [23]. Some studies also proposed for fatigue continuum damage models which, however, were based on rather simple or simplified tensorial damage behavior [24–27].

None of the aforementioned models are able to predict the Paris law exponent or the size effect. They all aim to describe the fatigue crack growth as a separate phenomenon and cannot realistically model concrete damage and failure in general situations where fatigue may be combined with general nonlinear triaxial behavior of concrete. To develop such a model is the objective of this article.

## 2. Formulation of constitutive model for fatigue damage

### 2.1. Overview of microplane model M7

Similar to Taylor models for polycrystalline metals [28–31], the basic idea of the microplane constitutive models, due to Taylor [32], is to express the constitutive law not in terms of tensors but in terms of the stress and strain vectors acting on generic plane of arbitrary orientation within the material, which is called the *microplane*. The use of vectors is conceptually simpler. It makes possible a semi-intuitive use of physical concepts such as frictional slip, microcrack opening and compression splitting (in the classical tensorial approach, the internal friction, for example, is represented by a relation between the first and second invariants even though it occurs only on planes of distinct orientation). Initially

the computational demands of the microplane model have been considered excessive, but with the current computer power microplane models have been run on systems of tens of millions of finite elements. Since computational demands of constitutive models increase with the structural system size linearly and those of system analysis quadratically, the difference between a simple tensorial constitutive model and the microplane model becomes negligible for very large systems.

In Taylor models, the stress vectors are assumed to be the projections of the stress tensor. However, this assumption would lead to instability in the case of strain softening. To ensure stable behavior, the microplane models consider a kinematic rather than static constraint of the microplanes, which means that the strain vector on the microplane is a projection of the strain tensor, and the stress tensor is obtained from the microplane stress vectors variationally, via principle of virtual work [33,34]. Also, in contrast to the Taylor models, the elastic deformation must, in the case of strain softening, be included on the microplane level. Considering the microplanes of all possible spatial orientations satisfies the tensorial invariance requirements. Capturing the interactions among various orientations makes the microplane model semi-multiscale in nature. Interactions at distance are, of course, not captured.

Microplane model M7 [35,36] is the latest version of progressively improved microplane models M1, M2, . . . , developed for concrete since 1985 [34,37]. Microplane models have also been developed for clays, soils, rocks, orthotropic foams, annulus fibrosus, shape memory alloy and fiber composites, both laminated (pre-preg or woven) and braided. Supplemented by a suitable localization limiter with a material characteristic length, such as the nonlocal model or the crack band model, model M7 has been shown to give very realistic response for a diverse range of loading conditions, including uniaxial, biaxial and triaxial loadings with post-peak softening, unconfined and confined compression, tension-shear failures, vertex effects when compression softening is followed by torsion [36,15], opening and mixed mode fractures, and compression-tension unloading and reloading up to a few cycles. What has been missing is the case of many cycles and fatigue loading, which is the objective of this study.

The basic mathematical structure of M7 is derived from thermodynamic potentials for three regimes, viz. elastic, damage and plastic-frictional. Stress-strain boundaries (or strain-dependent yield limits) are imposed on the microplanes. To distinguish between compression at low and high confinement, different boundaries are imposed on the volumetric and deviatoric compressive stresses on the microplanes. In addition, there is boundary on the tensile normal strains and a plastic-frictional boundary on the microplane shear stress depending on the normal stress and volume change. There are seven free, easily adjustable material parameters, which make it possible to match the given compressive strength, the corresponding strain, the given hydrostatic compression curve, and certain triaxial aspects. Besides, there are many fixed, hard-to-adjust, parameters, which are the same for all concretes. For details, see [35]. The numerical algorithm of M7 is explicit, and thus in each load step the stress tensor is obtained from the strain tensor, with no iterative loops. This makes the model robust and a suitable choice for large-scale finite element computations required for fatigue analyses.

## 2.2. Measure of cyclic damage

In microplane model M7, the elastic modulus  $E_N$  for the normal microplane strain  $\epsilon_N$  on microplane number  $\mu$  is assumed to undergo damage according to the equation:

$$\frac{E_N(\mu)}{E_{N0}} = \exp(-A\epsilon_N^{0+}(\mu)) \quad (2)$$

Here  $E_N(\mu)$  is the damaged normal modulus of the  $\mu$ th microplane,  $E_{N0}$  is the original undamaged modulus,  $A$  is a material constant (which is referred to as  $c_{13}$  in [35]) and  $\epsilon_N^{0+}(\mu)$  is the maximum strain reached so far on the  $\mu$ th microplane. This history dependence of the normal strain measure suffices for modeling only a few load cycles but is found to be insufficient for fatigue.

If used for more cycles, it does not predict the right trend of compliance evolution, and differs from the Paris law. To effectively predict the fatigue response under several hundreds or thousands of cycles, a new damage measure is proposed here.

It is expected that the accumulation of cracking damage during cyclic loading can be characterized by accumulated damage in the volumetric strain  $\epsilon_V$ . The cyclic damage measure, denoted as  $\zeta$ , can never decrease. It is calculated as the *path length* of the inelastic volumetric strain in the strain space. The path length, calculated separately for each material point, may be interpreted as an intrinsic time in the endochronic theory of inelastic behavior [38], which was used quite effectively for metals in [39] and for concrete in [38], though not at high numbers of cycles.

To describe this mathematically, consider a material point in cyclically loaded specimen, in a given load increment during a cycle, increasing or decreasing. Let  $d\epsilon_V$ ,  $d\epsilon_V^e$  and  $d\epsilon_V^i$  be the increments of total, elastic and inelastic volumetric strains, respectively. Therefore we have,  $d\epsilon_V = d\epsilon_V^e + d\epsilon_V^i$ . Now, if  $d\sigma_V$  is the increment of volumetric stress and  $K_b$  is instantaneous bulk modulus, we have  $d\epsilon_V^e = d\sigma_V/K_b$  (the suffix  $b$  is used to distinguish the bulk modulus from the stress intensity factor  $K$ ). Then, if  $\zeta_0$  is the damage parameter at the beginning of the increment, then the value  $\zeta$  at the end of the increment is given by

$$\zeta = \zeta_0 + d\zeta, \quad d\zeta = |d\epsilon_V^i| \quad (3)$$

The absolute value must be considered because the material undergoes irreversible damage even during the unloading part of the cycle, as evidenced from the experimental unload-reload response of concrete structures [10]. For ceramics, the damage during unloading was attributed to the reduction in fatigue crack shielding mechanisms in [8]. But the physical source of this behavior in concrete is not fully understood. In several existing formulations [20,21,40], the slope of the unloading branch had to be intuitively assumed to be somewhere between the elastic slope and the secant slope toward the origin. This, of course, introduces empiricism and takes away prediction capability. The microplane model automatically predicts this because even after the start of overall unloading, some microplanes are still loading and also because the newly introduced damage measure never decreases. Simulations with model M7 indicate that this fact suffices to capture, with no empirical assumptions, the essence of fatigue response, viz., the unloading-reloading hysteresis.

Furthermore, it is considered here that the cyclic damage accumulates only under tension and not under compression. The additional dissipative losses due to friction and slip under compression are accounted for automatically in the crack band by the inclined microplanes that are slipping under compression. On the other hand, in the model of [18] these losses are not automatic and had to be modeled separately by a contact constraint between the cohesive crack faces.

## 2.3. Instantaneous value of the bulk modulus $K_b$

Accurate representation of the increments of inelastic volumetric strain requires calculating the degradation of the instantaneous bulk modulus. It is intuitive to note that the degradation of normal microplane moduli  $E_N$  is related to the damaged macroscopic bulk modulus. This relationship will now be proven rigorously.

According to the virtual work principle applied to an elementary unit sphere of material (of volume  $4\pi/3$ ), the increment  $\Delta\sigma_V$

of volumetric stress  $\sigma_V$  is in equilibrium with the increments  $\Delta\sigma_N$  of microplane normal stresses  $\sigma_N$  if and only if

$$\frac{2\Pi}{3}\Delta\sigma_V\delta_{ij} = \int_{\Omega} \Delta\sigma_N N_{ij} d\Omega \quad (4)$$

where  $N_{ij} = n_i n_j$  (components of  $\mathbf{N} = \mathbf{n} \otimes \mathbf{n}$ ),  $n$  are the Cartesian components of normal microplane unit vector  $\mathbf{n}$  of unit hemisphere surface  $\Omega$  (for detail see [35]). Since  $\Delta\sigma_V = 3K_b\Delta\epsilon_V$  and  $\Delta\sigma_N = E_N\Delta\epsilon_N$ , we have

$$3K_b\Delta\epsilon_V\delta_{ij} = \frac{3}{2\pi} \int_{\Omega} E_N\Delta\epsilon_N N_{ij} d\Omega \quad (5)$$

This expression is non-zero only when  $i = j$ , and since  $N_{ii} = n_i n_i = 1$  and  $\delta_{ii} = 3$ , we get,

$$3K_b\Delta\epsilon_V = \frac{1}{2\pi} \int_{\Omega} E_N\Delta\epsilon_N d\Omega \quad (6)$$

Now,  $\Delta\epsilon_V = \frac{1}{3}\Delta\epsilon_{kl}\delta_{kl}$  and  $\Delta\epsilon_N = \Delta\epsilon_{kl}N_{kl}$ , and so

$$\left( K_b\delta_{kl} - \frac{1}{2\pi} \int_{\Omega} E_N N_{kl} d\Omega \right) \Delta\epsilon_{kl} = 0 \quad (7)$$

This is a variational equation that must hold for any  $\Delta\epsilon_{kl}$ , and so the term in the parenthesis must vanish. So,

$$K_b\delta_{kl} = \frac{1}{2\pi} \int_{\Omega} E_N N_{kl} d\Omega \quad (8)$$

Again, the above expression is non-zero only if  $k = l$ . Since  $N_{kk} = n_k n_k = 1$ , we finally obtain the instantaneous value of bulk modulus:

$$K_b = \frac{1}{6\pi} \int_{\Omega} E_N d\Omega \quad (9)$$

As a check, note that if  $E_N$  is the same for all the microplanes, which is the case for purely elastic case, Eq. (9) reduces to  $K_b = (E_N/6\pi) \int_{\Omega} d\Omega = E_N/3$  because  $\int_{\Omega} d\Omega = 2\pi$ , i.e., over the surface of a unit hemisphere. To evaluate this integral in a finite element program, one may use the optimal Gaussian numerical integration formula for a spherical surface, which reads:

$$K_b = \frac{2}{3} \sum_{\mu=1}^{N_{\mu}} w_{\mu} E_N(\mu) \quad (10)$$

where  $N_{\mu}$  is the number of microplanes; and  $E_N(\mu)$  and  $w_{\mu}$  are the normal modulus values and weights for microplanes with unit normals  $n_{\mu}$  specified by the Gaussian integration formula [34].

#### 2.4. Material softening law

The next step is to characterize the material stiffness degradation as a function of the accumulated damage. To achieve a model applicable to both cyclic crack growth and general nonlinear triaxial softening behavior, microplane model M7 needs to be extended to cyclic loading in a way that would not affect the previous calibration of M7 by triaxial data. Let the damage state of the material on a generic microplane be characterized by damage parameter  $\omega = E_N/E_{N0}$  such that  $\omega = 1$  in the undamaged state and  $\omega = 0$  in the fully damaged state. The existing softening law given by Eq. (2) can be rewritten as

$$\omega = \exp(-Ac_N^{0+}) \quad (11)$$

Now, let  $\omega_{cyc}$  be the material softening damage due to cyclic loading, characterized as  $\omega_{cyc} = f(\zeta)$  where function  $f(\zeta)$  needs to be found so as to simulate the Paris law for fatigue crack growth. So we generalize the last equation as,

$$\omega = \exp(-Ac_N^{0+})\omega_{cyc} = \exp(-Ac_N^{0+})f(\zeta) \quad (12)$$

To obtain the dependence of  $\omega$  on the path length  $\zeta$ , one may use an analogy with the Paris law, in which the rate of fatigue crack growth  $da/dN$  continuously increases in proportion to a power of  $\Delta K$ . Accordingly, the following continuously increasing rate of damage accumulation is introduced:

$$\frac{d\omega_{cyc}}{d\zeta} = -s\zeta^p \quad (13)$$

Here  $s$  and  $p$  are material parameters and the negative sign implies a decrease in  $\omega_{cyc}$  with an increase in  $\zeta$ . It should be noted that the rate of damage accumulation is defined with respect to  $\zeta$ , the internal time, and not the actual time or the cycle number. Thus the formulation is free from any explicit dependence on the cycle number, which is important when the cycles are non-periodic, with variable amplitudes and shapes. Now, we integrate the above power law, which gives

$$\omega_{cyc} = - \int s\zeta^p d\zeta = \bar{C} - \frac{s\zeta^{p+1}}{p+1} \quad (14)$$

where  $\bar{C}$  is the integration constant. It is evident, that the value of  $\bar{C}$  is equal to unity, since when  $\zeta = 0$ ,  $\omega_{cyc} = 1$ . Therefore we have,

$$\omega_{cyc} = 1 - r\zeta^q \quad (15)$$

where  $r = s/q$  and  $q = p + 1$ . (See Fig. 2, where  $r = 400$ ,  $q = 2$ ).

This function, though, must be modified for larger  $\zeta$  since  $\omega_{cyc}$  cannot become negative and must approach  $\omega_{cyc} = 0$  (total damage) asymptotically. Eq. (15) is equivalent to the function  $\omega_{cyc} = 1/x$  where  $x = (1 - r\zeta^q)^{-1}$ . Then, if  $x$  is expressed as a Taylor series as,  $x = 1 + r\zeta^q + r^2\zeta^{2q} + \dots$ , it satisfies the conditions  $\omega_{cyc} \geq 0$  and  $\lim_{\zeta \rightarrow \infty} \omega_{cyc} = 0$ . It is found that the data fits are satisfactory if the expansion of function  $x$  is truncated after the second term.

This leads to the function:

$$\omega_{cyc} = \frac{1}{1 + r\zeta^q + r^2\zeta^{2q}} \quad (16)$$

See the solid curve in Fig. 2, which shows  $\omega_{cyc}$  to approach zero asymptotically. Since  $\omega_{cyc} \approx 1$  for the first one or two cycles and sufficiently small  $r$ , the fits of the nonlinear triaxial test data will not be compromised. So the damage law generalized to fatigue finally reads as

$$\omega = \exp(-Ac_N^{0+}) \left( \frac{1}{1 + r\zeta^q + r^2\zeta^{2q}} \right) \quad (17)$$

### 3. Evaluation and validation of the model

To verify and calibrate the cyclic generalization, microplane model M7 is incorporated in the commercial finite element code ABAQUS (version 6.11), using the user defined explicit material subroutine VUMAT [41]. Since an important feature of quasibrittle materials is the size effect, fatigue tests of concrete with different specimen sizes are chosen. They are the three-point bend tests of concrete beams of normal strength and high strength reported in

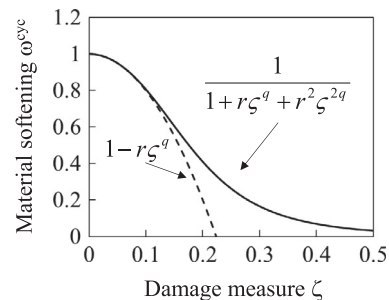


Fig. 2. Proposed material damage law.

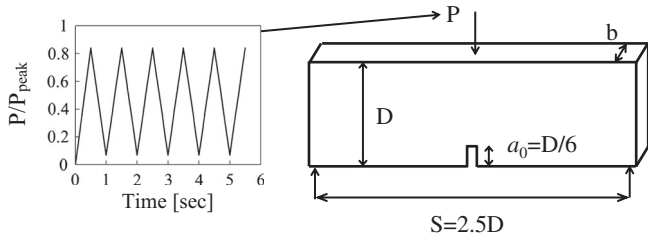


Fig. 3. Schematic of geometry and applied loading history.

[1,2], with three different sizes, similar in two dimensions; see Fig. 3. Since the model is intended to capture not only the cyclic crack growth but also the tensorial aspects of damage, the cohesive crack model is insufficient and either a nonlocal damage model or crack band model must be used to serve as localization limiter. We adopt the crack band model [14], whose usage in practice is by far the widest, because of its simplicity.

### 3.1. Finite element mesh for crack band model

The beams were meshed by eight-node hexahedral elements with reduced integration and hourglass stiffness [41]. Along the notch extension line, the mesh had a band of elements representing the advancing crack band (Fig. 4). To avoid spurious mesh sensitivity, the reference crack band width must be considered a material property, which represents the localization limiter and is chosen to be of the order of the aggregate size (it was 10 mm for the high strength concrete beams).

If the size of the elements in the crack band is changed, the post peak behavior must be scaled accordingly, so that the fracture energy would remain unchanged. An equivalent localization element effecting the scaling of postpeak behavior in arbitrary general situations of complex damage models, especially the microplane model, was developed in [15] (and has been used in the commercial code ATENA). It uses elastically unloading layers attached onto a core with softening damage in the principal stress directions. However, every scaling of the postpeak response introduces at least some numerical error, which might not be negligible when the stresses inside the FPZ are of interest. So, as far as possible, the crack band width should preferably be kept constant when the specimen size is varied, which is what is done here.

The use of microplane model is particularly helpful when the triaxial behavior in the FPZ is of interest. The reason is that, depending on the triaxial stress state in the FPZ, some microplanes

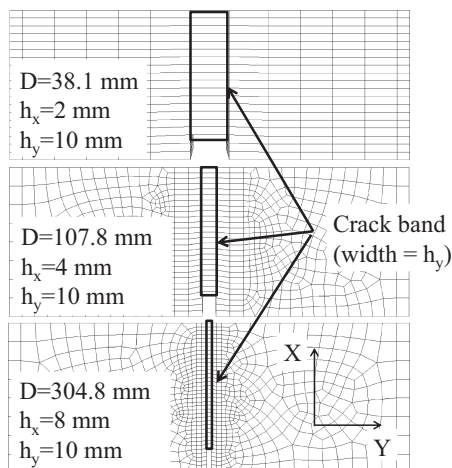


Fig. 4. Finite element meshes of the beams showing the crack band.

are still loading while others are unloading. It is this combination of loading and unloading on microplanes of different orientations that leads to the build-up of self-equilibrating residual stresses in the cyclic FPZ [37].

The width of the notch in the mesh must be the same as the crack band width. The bluntness or sharpness of the notch does not matter as long as the notch is not wider at its tip than about one third of the FPZ. Thus, in testing of metals or fine-grained ceramics, in which the FPZ size can be of micrometer dimensions, the sharpness of the notch is very important. But in concrete the FPZ width is of centimeter dimensions, and so the bluntness of the simulated notch is not a problem.

The restriction on element size is applicable only to the direction normal to crack growth plane (i.e.,  $h_y$  in Fig. 4). The mesh size in the direction of crack growth,  $h_x$ , does not appreciably affect the localization behavior. Therefore, to capture the stress profile in the crack band along the ligament of small specimen, the mesh can be refined in the crack growth direction as needed. For the high strength concrete beams, the element size in the growth directions is introduced as 2 mm for the small beams, 4 mm for the medium beams and 8 mm for the large beams, while the crack band width is 10 mm for all (Fig. 4).

Further, even though the beams are symmetric, we model the full specimen. Were only one half of the beam used, the post-peak response of the elements lying in the crack band along the centerline would have to be scaled to double the energy dissipation since one half of the crack band would give one half of the actual energy dissipated. Moreover, modeling the full beam allows the integration points in the crack band to be located exactly along the centerline, for any beam size. These and other numerical aspects of the crack band model are explored in detail in [42].

### 3.2. High strength concrete

The high strength concrete beams had a size ratio  $1 : \sqrt{8} : 8$  and their depths were  $D = 38.1, 107.8$  and  $304.8$  mm. All the beams had a span  $S = 2.5D$ , an initial notch of length  $a_0 = D/6$  and the width of 38.1 mm. The Young's modulus was  $E = 38.3$  GPa, Poisson's ratio  $\mu = 0.18$ , average compressive strength  $\bar{f}_c = 90.3$  MPa and density  $\rho = 2400$  kg/m<sup>3</sup>. The free parameters of the microplane model [36] were calibrated to match the peak loads of the three beams from monotonic loading tests (the full load–displacement curve could also be used for calibration but was not reported). Only the radial scaling parameter  $k_1$  (defined in [36]) had to be adjusted in order to predict the peak loads for the beams within acceptable error; its value came to be  $k_1 = 150 \times 10^{-6}$ . All the other parameters of the model were equal to their default values listed in [36]. The predicted peak loads showing good agreement with the corresponding values from experiments are shown in Table 1.

Using the calibrated extended microplane model, fatigue simulations have been performed on the three beams, using a high-performance parallel computing (HPC) cluster system at Northwestern University (called QUEST [43]). The applied cyclic loading had maximum and minimum load limits corresponding 84% and 7% of peak load. The load frequency was 1 Hz, which ensured absence of inertia effects.

Table 1  
Experimental and predicted peak loads for beams from [2].

Beam size $D$ (mm)	Test avg (MPa)	Predicted by M7 (MPa)	% error
38.1	7.53	7.06	−6.14
107.8	5.4	5.22	3.32
304.8	3.72	3.87	4.12

**Table 2**  
Experimental and predicted fatigue lifetimes for beams from [2].

Beam size $D$ (mm)	Test lifetime (Specimen 1)	Predicted lifetime
38.1	212	217
107.8	854	189
304.8	1348	170

### 3.2.1. Fatigue lifetime

In the actual tests, the lifetime of the small beam was 212 cycles under this applied load. Data on only one specimen were available. So, the damage law parameters were adjusted until the lifetime prediction was close enough. For  $r = 1600$  and  $q = 2$ , the model predicted failure in 217 cycles, which is a very good agreement. In the terminal cycle, failure is manifested by a sudden increase, by several orders of magnitude, of the overall deformation.

Table 2 shows a summary of the predicted and observed lifetimes for beams of all three sizes. Since parameters  $r$  and  $q$  were adjusted to match the lifetime of the small beam exactly, there is some disagreement for medium and large sizes. Moreover, the test data show an increase of the lifetime with the beam size but the simulations show a decrease. However, the increase might be a chancy result of only one test per size. Intuitively, the lifetime decrease is expected since larger structures are more brittle. The decrease is also consistent with the probabilistic theory in [44], where a lifetime decrease with increasing size is predicted for both static and cyclic crack growths. Generally, the scatter in fatigue

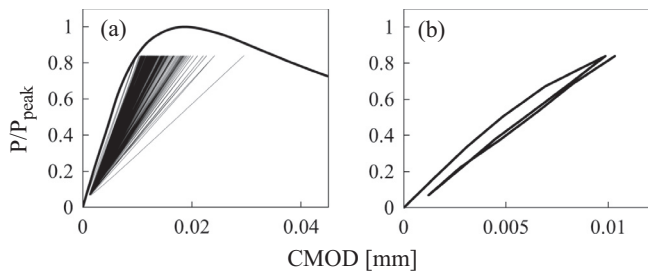


**Fig. 5.** Load CMOD curve from M7 simulations showing unloading reloading hysteresis for the small beam. (a) Entire lifetime. (b) First cycle.

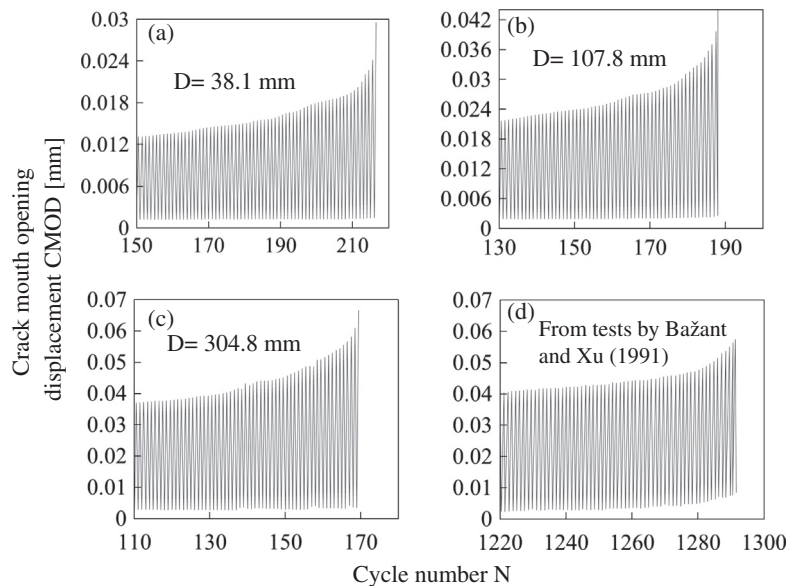


**Fig. 6.** Evolution of CMOD. (a) Small beam. (b) Medium beam. (c) Large beam. (d) Experimental data.

lifetimes is known to be extremely variable, spanning even two orders of magnitude. This is further enhanced by the uncertainty in the applied load due to lack of a priori knowledge of the structure strength.

Furthermore, note that the lifetime is controlled not only by damage but also by the evolution of the energy release rate (or the stress intensity factor) as the crack is growing. This can have a large and size-dependent effect on the lifetime if the crack extension is not negligible compared to the length of the notch and of the ligament. Therefore, differences in experimental lifetimes smaller than an order of magnitude cannot be taken too seriously if only single tests are available. The scaling aspect in fatigue of quasibrittle materials will be considered in detail in a subsequent article.

Besides, note that the present results are obtained with a deterministic model in which the material properties are uniform throughout the structure. This cannot predict more than the mean behavior. The randomness of the problem could possibly be simulated by randomizing the material property fields (the modulus and strength boundaries, and possibly also the fatigue damage parameters ( $r$  and  $q$ ), but this has yet not been explored).

### 3.2.2. Unloading–reloading hysteresis

To evaluate the predicted unloading–reloading hysteresis, the load is plotted versus the crack mouth opening displacement, CMOD. The CMOD values are stored at the peak and valley for each load cycle. In Fig. 5, they are plotted against the load for the complete lifetime. It is seen that the slope of the unloading arm continuously decreases. In every cycle, the new CMOD peak is higher than the previous peak. This is shown more clearly for the first cycle in Fig. 5b. The load vs. CMOD curve for the monotonic loading case is also plotted. It may be noted that the monotonic response acts as the envelope of the cyclic response.

Fig. 6a–c show the CMOD evolution for all three sizes in the final 80–100 cycles before failure. A similar result from [1] is shown in Fig. 6d, but only for a qualitative comparison since the cycle by cycle CMOD data were not reported for this data set. Note that, in agreement with tests, the predicted CMOD growth is initially slow, but becomes much quicker towards the end. The trend predicted for all the sizes agrees very well with the tests, especially the CMOD growth at maximum load. These results also agree well

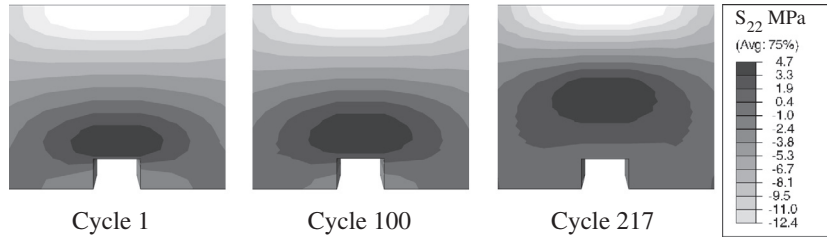


Fig. 7. Various stages of predicted cyclic FPZ.

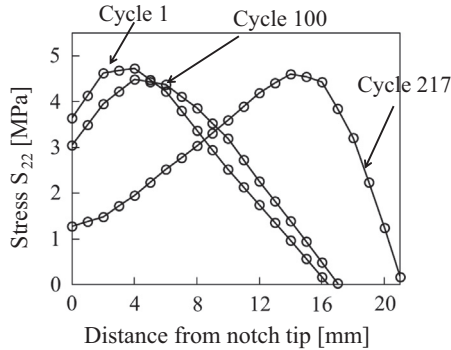


Fig. 8. Evolution of the predicted stress profile in the cyclic FPZ.

with other experiments [17,23] and verify that the model describes well the essential features of fatigue.

3.2.3. Sub-critical fatigue crack propagation

Fig. 7a–c show three stages of the cyclic FPZ in the simulation of the small beam, viz. the formation, detachment and propagation. The FPZ is visualized via a contour plot of the stress in the y-direction or  $S_{22}$  (normal to the notch direction) at maximum load in cycles 1, 100 and 217. The corresponding stress profile in the crack band at maximum load in these cycles is shown in Fig. 8. The FPZ is seen to develop around the notch tip in the first cycle itself. When the maximum load is reached, the maximum stress is actually at a small distance away from the notch tip (not at the tip), indicating that some softening has already taken place in this region.

With continued cycling, the near tip region softens further, thereby causing a slow increase in the compliance of the structure. This continues until about the 100th cycle, at which point there is sufficient local softening so as to cause the stress peak to move away from the tip. In Fig. 7b this is seen as the detachment and movement of the FPZ away from the tip, essentially implying sub-critical growth of the fatigue crack. The term ‘sub-critical’ indicates that crack growth occurs at stress intensity factors ( $K_I$ ) that are smaller than the critical  $K_{IC}$  for monotonic loading. For structures of positive geometry, which is the present case, crack growth

causes  $K_I$  for increase. More and more elements in the crack band continue to undergo softening and the FPZ moves farther away from the notch tip. Finally, once the FPZ has moved by a critical distance at which  $K_I$  has grown to its critical value  $K_{IC}$  (Fig. 7c), stability is lost and the structure fails dynamically. In this particular simulation, this occurred during the 217th cycle.

For further explanation, the damage variable  $\zeta$  and the degree of cyclic damage  $\omega_{cyc}$  are plotted in Fig. 9a and b against the cycle number, for the first four elements in the crack band. The elements are labeled 1 through 4, with element 1 being the closest to the notch tip. Although the applied load is cyclic, the damage measure  $\zeta$  increases continuously, as the damage accumulates during both loading and unloading. In any given cycle, the value of  $\zeta$  in element 1 is the highest, progressively decreasing as the crack growth. The trend of the FPZ growth and damage evolution is similar beams of all sizes.

3.2.4. Sub-critical fatigue crack length

For quasibrittle fracture in concrete type materials, the material heterogeneity and the diffuse character of microcracking at the crack front make optical or acoustical determination of the effective crack length impossible. The linear elastic fracture mechanics (LEFM) is inapplicable and one must use the equivalent LEFM approximation [10], in which the effective crack length considered as  $a = a_0 + c_f$ , where  $a_0$  is the length of the traction free crack;  $c_f$  is approximately equal to half the FPZ length and is defined precisely by specimen stiffness (an exact ratio of  $c_f$  to Irwin’s characteristic length  $l_0$  is derived in [45]). The effective length of the growing crack is thus measured indirectly by the compliance method, in both experiment and calibration.

The CMOD compliance values  $C_{CMOD}$  are defined as the unloading slopes on the load vs. CMOD plot. For various values of the notch length  $a_0$ , the CMOD compliance is calculated by simulating one loading cycle at a very low maximum load. Then, a cubic polynomial is obtained by regression, to relate  $C_{CMOD}$  and  $a_0$ . This process is repeated for each beam size.

To determine evolution of the sub-critical fatigue crack length, first the  $C_{CMOD}$  is calculated in each cycle as the inverse slope of the unloading segment of the load-CMOD curve (Fig. 5). When

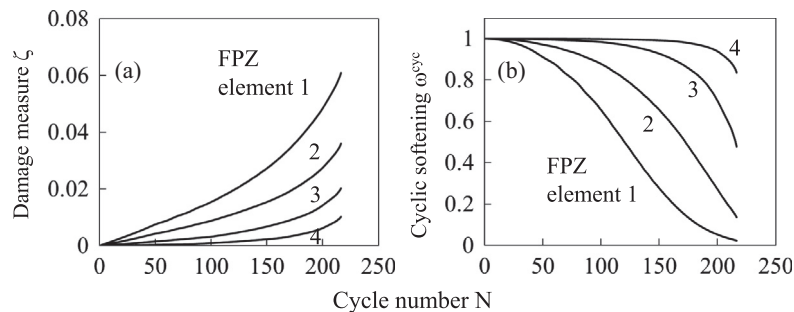


Fig. 9. Evolution of (a) damage measure  $\zeta$  (b) degree of material softening due to cycling  $\omega_{cyc}$ .

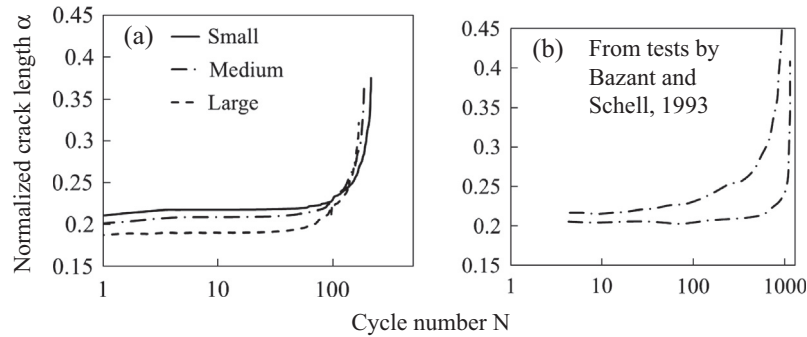


Fig. 10. Evolution of normalized crack length. (a) Predicted (all 3 beams). (b) Typical curves from experiments.

substituted into the previously fitted calibration polynomial, this compliance provides the effective crack length in that cycle. The crack length normalized by the structure size  $D$  is denoted as  $\alpha$  and is plotted in Fig. 10a vs. the cycle number  $N$ , for all three beams. For comparison, the typical curves from the experiments are shown in Fig. 10b [2]. Again, the predicted trend of crack growth agrees quite well with the test data. It is seen that the crack growth is slow initially, and then becomes more and more rapid towards final failure. The point at which the rate of crack growth suddenly curves upwards also corresponds to when the FPZ detaches from the notch tip. These plots further verify the predictive capabilities of the model.

### 3.3. Normal strength concrete

Similar simulation results were obtained for the tests of normal strength concrete beams reported in [1]. These beams had a size ratio of 1 : 2 : 4. (See Fig. 3) and the sizes  $D$  of the small, medium and large beams were 38.1, 76.2 and 152.4 mm, respectively. All the beams had a span  $S = 2.5D$  and width of 38.1 mm. The initial notch depth was  $a_0 = D/6$ . The finite element mesh was similar to that shown in Fig. 4 for high strength concrete beams. The crack band width was considered as 10 mm, which is approximately equal to the maximum aggregate size. The Young's modulus was  $E = 27.12$  GPa, Poisson's ratio  $\mu = 0.18$ , mean compression strength  $\bar{f}_c = 32.8$  MPa, and density  $\rho = 2400$  kg/m<sup>3</sup>.

To match the monotonic loading response within acceptable error, only the radial scaling parameter  $k_1$  had to be adjusted ( $k_1 = 140 \times 10^{-6}$ ). All the other parameters of the model were equal to their default values listed in [36].

The calibrated monotonic response of all three beams is compared against the experimental data in Fig. 11, which shows

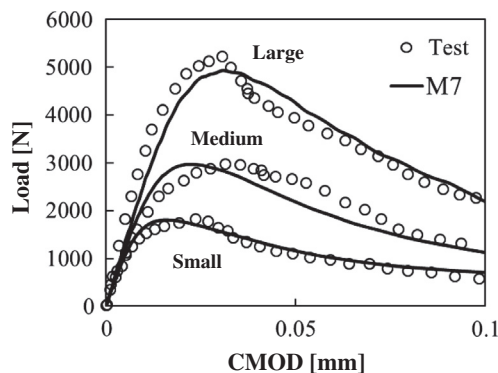


Fig. 11. Comparison of monotonic response of beams from [1] predicted by M7 with experiments.

good agreement. The calibrated model was then used to perform simulations of fatigue crack growth on the beams with maximum and minimum loads equal to 80% and 0% of the monotonic peak load, as used in the tests. The frequency in simulations was 1 Hz, which was slightly higher in actual tests, but was still sufficiently low to allow quasi-static calculations. The relevant damage law parameters were  $r = 750$  and  $q = 2.5$ . These were optimized so as to obtain both the right lifetime and the right crack growth rate.

Table 3 shows the predicted and observed lifetimes for the beams of all three sizes and, again, the predictions agree with the data. Here, the experimentally observed lifetimes show almost no size effect, but the simulations consistently predict decreasing lifetime with increasing size.

The normalized effective crack length  $\alpha$  was determined for each size by means of the compliance calibration method, as described before. Fig. 12 shows a comparison of the predicted and experimentally obtained values of  $\alpha$  plotted against the cycle number  $N$  for all three beams. The figure shows the agreement to be quite satisfactory. Consistent with previous results, the predicted and observed crack growth rates are slow initially, but rapidly accelerate towards the end. The acceleration is not only a material property but is caused mainly by the growth of effective  $K_I$  as the crack extends. These comparisons indicate that the sub-critical fatigue crack growth in both normal and high strength concrete is predicted by the model realistically.

## 4. Paris law

The Paris law [3], Eq. (1), originally established empirically and recently justified theoretically (based on probabilistic nano-mechanical arguments [44]), is the most widely used relation for fatigue crack growth. A complete Paris law plot extends beyond the power-law range and typically has the sigmoidal shape shown in [4]. Thus the initial and final parts of the simulated plots lie outside the Paris' power-law regime. The initial part represents a very slow crack growth, below the threshold of power law, and the final part represents accelerating growth toward failure. The central linear part of the plot represents the Paris' power law. Concrete and some other other quasi-brittle materials such as tough ceramics are known to have a high Paris law exponent, about 10–50. A physical justification for this high value was provided using atomistic arguments and multi-scale transitions in [44].

Table 3  
Experimental and predicted fatigue lifetimes for beams from [1].

Beam size $D$ (mm)	Test lifetime (Specimen 1)	Test lifetime (Specimen 2)	Predicted lifetime
38.1	974	939	848
76.2	850	1286	768
152.4	882	1083	755

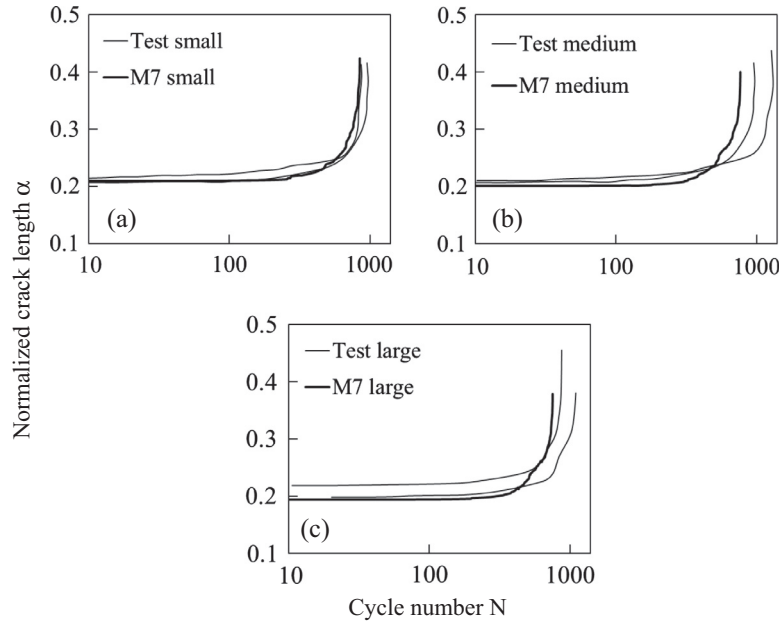


Fig. 12. Evolution of normalized crack length (Predicted and measured). (a) Small size. (b) Medium size. (c) Large size [1].

So far it has been shown that the present model is capable of predicting the form of the crack growth curve. But it is important to predict also the right exponent of Paris law. Such a prediction, which has been made only in a few studies, e.g., [18,46], provides a challenging, though stringent, check on the capability of the model.

4.1. High strength concrete

First let us consider the Paris law prediction for high strength concrete, as described in Section 3.1. The crack lengths  $a = D\alpha$  calculated from compliance calibration were used to obtain the rate of crack growth in terms of the number of cycles, i.e.,  $\Delta a/\Delta N$

(the rate was computed using  $\Delta N = 5$ ). Further, the mode-I stress intensity factor  $K_I$  was calculated as,

$$K_I = \frac{P}{b\sqrt{D}}f(\alpha) \tag{18}$$

where  $P$  = applied load,  $b$  = thickness of the beam,  $D$  = depth of the beam taken as its size, and  $f(\alpha)$  = dimensionless stress intensity factor as a function of  $\alpha$ . For the present geometry [2]:

$$f(\alpha) = \frac{6.647\alpha^{1/2}}{(1-\alpha)^{3/2}}(1 - 2.5\alpha + 4.49\alpha^2 - 3.98\alpha^3 + 1.33\alpha^4) \tag{19}$$

For every calculated value of crack length  $\alpha$ ,  $K_{max}$  and  $K_{min}$  are calculated using Eqs. (18) and (19). The difference gives the amplitude

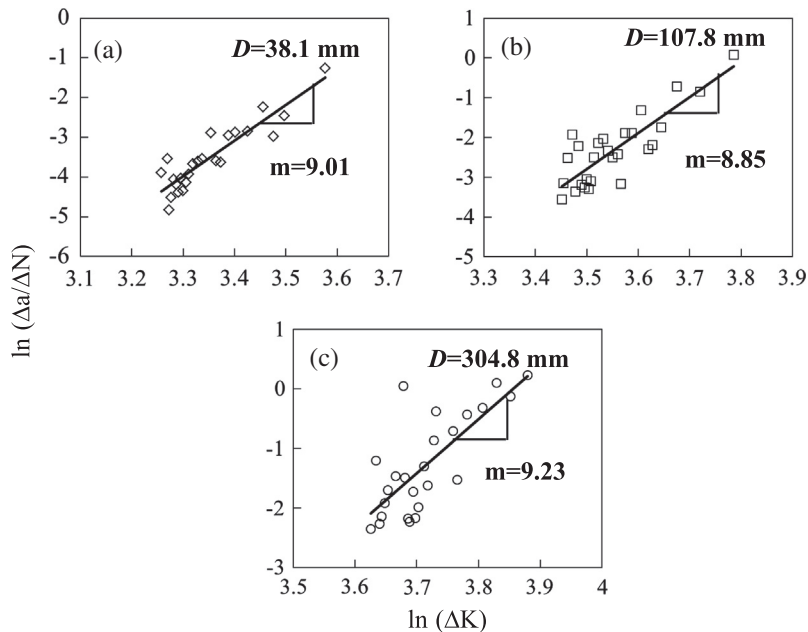


Fig. 13. Predicted Paris law for high strength concrete. (a) Small beam. (b) Medium beam. (c) Large beam.

**Table 4**  
Experimental and predicted Paris law parameters for beams from [2].

Beam	ln C		m	
	Test	M7	Test	M7
Small	-33.67	-33.78	8.44	9.01
Medium	-35.61	-34.4	8.57	8.85
Large	-36.7	-34.82	9.61	9.23

$\Delta K$ , and is plotted on a log–log plot, against  $\Delta a/\Delta N$  in Fig. 13a for the small beam of high strength concrete (from Section 3.1).

The resulting plot resembles a typical Paris law plot including the initial slow crack growth regime followed by a regime of stable crack growth (shown by small diamonds). When the amplitude,  $\Delta K$ , reaches the critical value ( $K_{IC}$ ), the third regime begins. The crack grows dynamically which is manifested in the model as collapse. The points for the dynamic growth are not a material property and thus are not included in the plot.

As seen, a straight line, whose slope is the Paris exponent  $m$ , is fitted only through the stable crack growth regime (or the Paris regime), since the final acceleration is not a material property. Here, the calculations yield  $m = 9.01$ . The tests of this beam yielded  $m = 8.44$ . This is a relatively good agreement, which suggests that Eq. (16) is realistic. Obviously, the present model is able to capture the high exponents  $m$  typical of quasibrittle materials.

By a similar calculation, the Paris law exponent is predicted for the medium and large size beams, as shown in Fig. 13b and c. The predicted and experimental values of ln C and  $m$  from the individual best fits are shown in Table 4 for all three beam sizes. As seen, the  $m$  values match the data well. The average  $m$ -value from the experiments is 8.60 while from the simulations it is 9.03.

The agreement in the Paris law coefficient C is also good, especially for the small-size beam. This is no surprise, since the lifetime calibration was performed on that beam. The reason why the predicted C values are lower than the experimental values for the medium- and large-size beams must be that the predicted lifetimes were correspondingly shorter. Nevertheless, the trend of scaling in C is consistent. The large scatter in experimental fatigue lifetimes

also causes scatter in the value of C. By contrast, the more important parameter, exponent  $m$ , is relatively unaffected by the scatter.

4.2. Normal strength concrete

Although similar tests of normal strength concrete have been carried out [1], only the number of cycles to failure and the measured slope of the Paris law plot, giving exponent  $m$ , can be used from these tests since an error in copying the formula for  $K_I$  from the literature has been detected. Accordingly, the Paris law plots are generated for all three normal strength concrete beams, from the simulations discussed in Section 3.2.

The damage law parameters are  $r = 750$  and  $q = 2.5$  (this optimum value of  $q$  differs from the optimum found for high strength concrete, which was 2.0). The optimum value of  $r$  had to be also adjusted, to match the observed number of cycles to failure. The Paris law exponent is obtained for each beam separately by fitting the linear segments of the data plots in Fig. 14. The values are shown in Table 5. The average exponent predicted from the model is  $m = 10.02$ , which is close to the experimental value of 10.60 and serves as another validation of the model. It is thus demonstrated that, with adjusted parameters, the proposed model predicts well the rate of sub-critical fatigue crack growth for both normal and high strength concrete.

4.3. Sensitivity to damage law parameters

The Paris law exponent and fatigue lifetime were seen to depend on parameters  $r$  and  $q$ . Furthermore they also depend on parameter A in Eq. (17), which coincides with one basic parameter of the microplane model and is a material property that must be

**Table 5**  
Experimental and predicted Paris law exponent for beams from [1].

Beam size	Test	M7
Small	11.78	9.84
Medium	9.97	10.05
Large	9.27	10.18

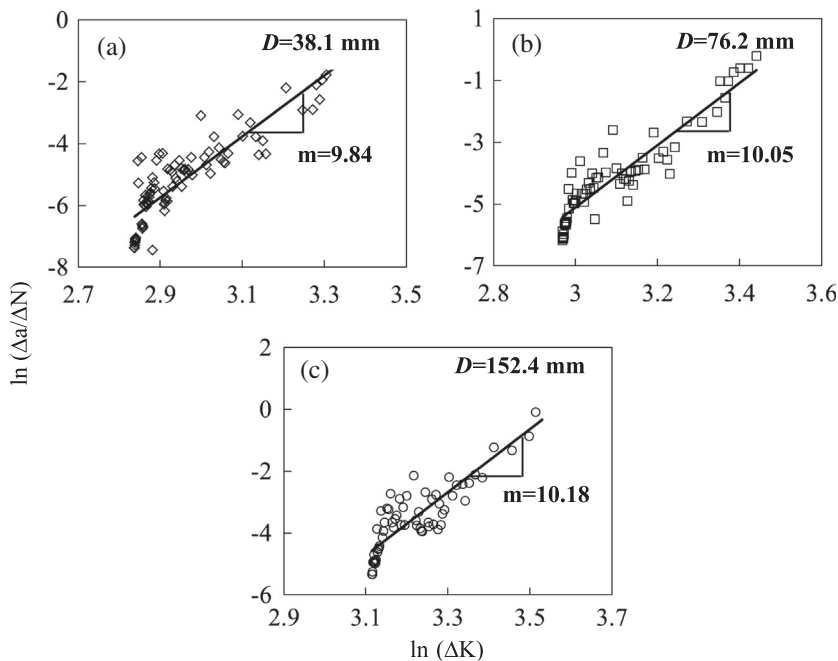


**Fig. 14.** Predicted Paris law for normal strength concrete. (a) Small beam. (b) Medium beam. (c) Large beam.

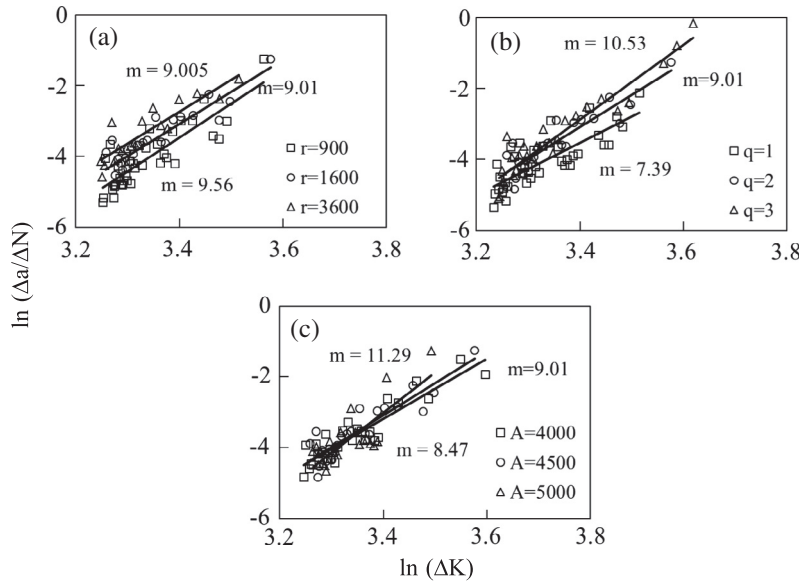


Fig. 15. Effect of parameter (a)  $r$ , (b)  $q$  (c)  $A$  on Paris law.

kept constant for the same type of concrete. To check the model sensitivity to these three parameters, fatigue simulations were performed on the small beam from [2] for the same loading as in Section 3.1 and for the various values of  $r$ ,  $q$  and  $A$ . Fig. 15a shows the Paris law plot for various values of  $r$  at fixed  $q=2$  and  $A=4500$ ; Fig. 15b for various values of  $q$  at fixed  $r=1600$  and  $A=4500$ ; and Fig. 15c for various values of  $A$  at fixed  $r=1600$  and  $q=2$ . The following observations can be made:

1. The value of  $r$  does not have a very strong effect on the predicted Paris law exponent  $m$ . However it does have an effect on the number  $N$  of cycles to failure. E.g., when  $r$  is decreased from 1600 to 900,  $N$  increases from 217 to 308, while  $m$  changes from 9 to 9.56. When  $r$  is increased to 3600,  $N$  decreases to 144 while  $m$  remains almost the same; see Fig. 15a.
2. Parameter  $q$  is seen to affect the Paris law exponent significantly. Decreasing  $q$  from 2 to 1 lowers  $m$  from 9.01 to 7.39, while  $N$  drops from 217 to 193. Increasing  $q$  to 3 increases the Paris law exponent to 10.53 and  $N$  to 228; see Fig. 15b.
3. Parameter  $A$  influences both  $N$  and  $m$ . Decreasing  $A$  from 4500 to 4000 changes  $N$  from 217 to 272 and  $m$  from 9.01 to 8.47. Increasing  $A$  to 5000 changes  $N$  to 168 and  $m$  to 11.29; see Fig. 15c.

Thus  $r$  affects mainly lifetime  $N$ , and  $q$  mainly Paris law exponent  $m$ . Parameter  $A$  affects both significantly. The effects of  $r$  on  $m$  and of  $q$  on  $N$  are secondary. These observations facilitate tuning the model to known  $N$  and  $m$ .

### 5. Sudden overload and residual strength

The present fatigue model is an integral part of a realistic, extensively verified, three-dimensional material constitutive model for damage, the microplane model M7. This makes it possible to predict two important phenomena: (1) the strength under sudden overload, and (2) the effect of non-fatal overload on the subsequent number of cycles to failure. Consideration of overloads is important for determining how the structure strength degrades with load cycling [47]. Without analysis of the overloads, the safety factors may be set uneconomically large or dangerously low.

#### 5.1. Sudden overload

The overloads during load cycling affect concrete differently from metals. In metals, they slow down the crack growth, due to formation of a plastic zone around the fracture process zone, which is an effect modeled in [18]. In concrete, the opposite is seen. A sudden overload accelerates the subsequent crack growth, since the fracture process zone suffers additional damage [46,48].

To study this phenomenon, the experiments reported in [46] are used. The load history consisted of periods of 500 cycles at constant amplitude each but after every 500 cycles the maximum load was suddenly increased. Here a similar load history is simulated numerically, except that the maximum load is increased after every 100 cycles since only a qualitative comparison is sought. From the numerical results, the effective crack length is

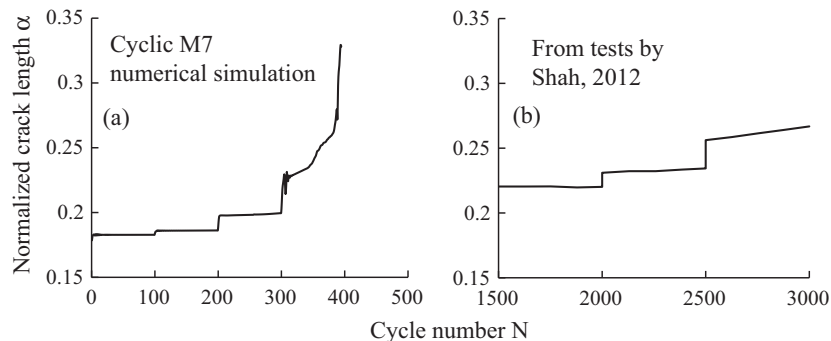


Fig. 16. Effect of sudden overload on fatigue crack growth. (a) Predicted. (b) Typical curve from experiments by Shah.

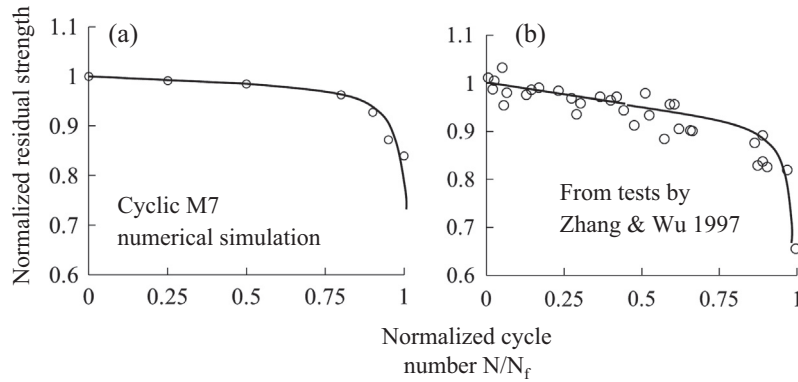


Fig. 17. Residual strength degradation curve. (a) Predicted. (b) Typical curve from experiments by Zhang and Wu.

calculated for every cycle and is plotted against the cycle number  $N$ , as shown in Fig. 16a.

Fig. 16b shows the results of experiments. Note that at the instant of sudden overloads, the crack length suddenly increases. This is due to a sudden increase of the damage parameter  $\zeta$ , and also of the damage variable  $\epsilon_{N0}^*$ , which further causes a sudden softening of the FPZ and a corresponding increase in compliance and effective crack length. This behavior is consistent with the trend of experimental data, and indicates that the present model is able to capture the increased sensitivity of the FPZ in concrete structures to sudden overloads. Further this demonstrates that the model is applicable to variable and random amplitude loadings as well.

### 5.2. Residual strength of the structure

Further it is necessary to compare, at least qualitatively, the predicted degradation of the residual strength of a structure to the experimentally obtained strength degradation curve. Fatigue simulations of varying duration were performed for small high-strength concrete specimens. The overload times were  $0.25N_f$ ,  $0.5N_f$ ,  $0.8N_f$ ,  $0.9N_f$  and  $0.95N_f$ . The calculated residual strength of the degraded specimen,  $\sigma_R$ , was normalized by the initial strength  $\sigma_N$ . The strength degradation curve obtained from the data, i.e., the plot of the normalized residual strength vs. the number of cycles (normalized relative to the lifetime), is plotted in Fig. 17a. Fig. 17b shows a similar degradation curve reported for concrete in [49]. Again, a good qualitative agreement with the data is demonstrated. This predicted trend is also consistent with the trend of degradation reported in [50,47], which indicates negligible degradation initially and rapid later on, doubtless caused by the growth of fatigue crack. The predictions also satisfy the condition that  $\sigma_R = \text{maximal applied load}$  when  $N=N_f$ . Practical applicability of the present model is thus demonstrated.

## 6. Conclusions

1. The microplane constitutive damage model developed here gives realistic predictions of fatigue crack growth in normal and high strength concretes up to several thousands of load cycles. Thus one gains, apparently for the first time, a general model that can realistically describe both the fatigue crack growth and the nonlinear triaxial damage behavior of concrete. This is important for practical applications to quasibrittle materials in which both the fatigue and arbitrary triaxial damage occur simultaneously (and may be expected to have implications for fatigue of large composite parts, micrometer scale devices, etc.).
2. Simulating the fatigue degradation and hysteresis by a new softening law in terms of the path length of the inelastic

volumetric strain in the strain space allows good agreement with previous experiments whose lifetimes were of the order of one-thousand cycles.

3. This agreement is achieved without any empirical assumptions about the form of the unloading–reloading curves other than the assumptions already present in microplane model M7. Thus it may be expected that the model is not limited to fixed amplitude loading, nor loadings with no rotation of principal stress directions.
4. The model presented captures well the gradual increase of the compliance of the structure caused by the fatigue crack growth.
5. The model can also distinctly identify the three phases during the travel of large fracture process zone—the formation, detachment and propagation of this zone. The model can be tuned to simulate correctly the evolution of the effective crack length during fatigue and the lifetimes registered in previous experiments.
6. The model is shown to capture the Paris law behavior accurately. It can simulate the initial regime of slow crack growth and the subsequent regime of stable fatigue crack growth. With an appropriate selection of the exponents in the proposed softening law, a high Paris law exponent, seen in quasibrittle materials, is captured well.
7. The model parameters are tunable to obtain varying Paris law exponents, thus making it suitable for adaptation to other quasibrittle materials such as rocks and ceramics.
8. The model can correctly predict the response of concrete under sudden overloads, thus making it suitable to study the response under variable amplitude loading. It can also predict correctly the residual strength degradation during cyclic loading, consistently with experiments.
9. Since the microplane model automatically exhibits the size effect, the present model may be expected to exhibit it, too, in the case of fatigue loading (this expectation will be checked in the subsequent paper). Also the size effect in fatigue, a relatively less understood aspect of scaling, can be studied in detail using this model.
10. Although the model has not yet been evaluated for fatigue failure due to crack initiation from a smooth surface, it is of interest for this important case, particularly for understanding the differences in strength scaling of notched and unnotched structures. These are topics of on-going research.
11. With mesh refinements and the nonlocal damage approach, the present fatigue microplane damage model may be expected to allow simulating the development of residual stresses and the changes of width and length of the fracture process zone during fatigue.

Note: For extension to high-cycle fatigue, with millions of load cycles, it will be necessary to formulate extrapolations using some sort of a cycle jump algorithm, as in [51].

## Acknowledgment

Financial support by the U.S. National Science Foundation under Grant CMS-0556323 to Northwestern University is gratefully acknowledged. Thanks are due to Ferhun Caner, associate professor at UPC, Barcelona, and Visiting Scholar at Northwestern University, for making available his coding of material subroutine for microplane model M7.

## References

- [1] Bažant ZP, Xu K. Size effect in fatigue fracture of concrete. *ACI Mater J* 1991;88(4):390–9.
- [2] Bažant ZP, Schell WF. Fatigue fracture of high-strength concrete and size effect. *ACI Mater J* 1993;90(5):472–8.
- [3] Paris P, Erdogan F. A critical analysis of crack propagation laws. *J Basic Eng* 1963;85:528–34.
- [4] Suresh S. *Fatigue of materials*. Cambridge: Cambridge University Press; 1991.
- [5] Ritchie RO. Cyclic fatigue crack growth in a SiC whisker-reinforced alumina ceramic composite: long and small crack behavior. *J Am Ceram Soc* 1992;75(4):759–71.
- [6] Liu SY, Chen IW. Fatigue of yttria-stabilized zirconia: I, fatigue damage, fracture origins, and lifetime prediction. *J Am Ceram Soc* 1991;74(6):1197–205.
- [7] Le J, Manning J, Labuz J. Scaling of fatigue crack growth in rock. *Int J Fatigue* 2013.
- [8] Ritchie RO. Mechanisms of fatigue-crack propagation in ductile and brittle solids. *Int J Fract* 1999;100:55–83.
- [9] Rice J. Mechanics of crack tip deformation and extension by fatigue. *Am Soc Test Mater* 1967;415:247–311.
- [10] Bažant ZP, Planas J. *Fracture and size effect in concrete and other quasibrittle materials*. CRC Press; 1998.
- [11] Barenblatt GI. The mathematical theory of equilibrium of cracks in brittle fracture. *Adv Appl Mech* 1962;7:55–129.
- [12] Dugdale DS. Yielding of steel sheets containing slits. *J Mech Phys Solids* 1960;8:100–8.
- [13] Hillerborg A, Modeer M, Petersson PE. Analysis of crack formation and crack growth in concrete by means of fracture mechanics and finite elements. *Cement Concr Res* 1976;6:773–82.
- [14] Bažant ZP, Oh BH. Crack band theory for fracture of concrete. *Mater Constr* 1983;16(3):155–77.
- [15] Červenka J, Bažant ZP, Wierer M. Equivalent localization element for crack band approach to mesh-sensitivity in microplane model. *Int J Numer Meth Eng* 2005;62(5):700–26.
- [16] Bažant ZP, Belytschko TB. Wave propagation in strain softening bar: exact solution. *J Eng Mech ASCE* 1985;111:381–9.
- [17] Gylloft K. A fracture mechanics model for fatigue in concrete. *Mater Constr* 1984;17(97):55–8.
- [18] Nguyen O, Repetto EA, Ortiz M, Radovitzky RA. A cohesive model of fatigue crack growth. *Int J Fract* 2001;110:351–69.
- [19] Elias J, Le J-L. Modeling of mode-I fatigue crack growth in quasibrittle structures under cyclic compression. *Eng Fract Mech* 2012;96:26–36.
- [20] Yang B, Mall S, Ravi-Chandar K. A cohesive zone model for fatigue crack growth in quasibrittle materials. *Int J Solids Struct* 2001;38:3927–44.
- [21] Horii H, Shin HC, Pallewatta TM. Mechanism of fatigue crack growth in concrete. *Cem Concr Compos* 1992;14:83–9.
- [22] Bahn BY, Hsu CT. Stress strain behavior of concrete under cyclic loading. *ACI Mater J* 1998;95-m18:178–93.
- [23] Hordijk D, Reinhardt H. Growth of discrete cracks under fatigue loading. In: Shah S, editor. *Toughening mechanisms in quasi-brittle materials*. Dordrecht; 1991. p. 541–54.
- [24] Peerlings RHJ, Brekelmans WAM, de Borst R, Geers MGD. Gradient-enhanced damage modelling of high-cycle fatigue. *Int J Numer Meth Eng* 2000;49:1547–69.
- [25] Desmorat R, Ragueneau F, Pham H. Continuum damage mechanics for hysteresis and fatigue of quasi-brittle materials and structures. *Int J Numer Anal Meth Geomech* 2007;31(2):307–29.
- [26] Kim Y, Allen DH, Little DN. Computational model to predict fatigue damage behavior of asphalt mixtures under cyclic loading. *J Trans Res Board*. Washington (DC): Transportation Research Board of the National Academies; 2006. p. 196–206.
- [27] Benjamin R, Ragueneau F. Continuum damage mechanics based model for quasi brittle materials subjected to cyclic loadings: formulation, numerical implementation and applications. *Eng Fract Mech* 2013;98:383–406.
- [28] Batdorf S, Budianski B. A mathematical theory of plasticity based on the concept of slip. Technical note 1871. Washington (DC): Nat Advisory Committee for Aeronautics; 1949.
- [29] Asaro RJ, Rice JR. Strain localization in ductile single crystals. *J Mech Phys Solids* 1977;33:309–38.
- [30] Manonukul A, Dunne FPE. High and low-cycle fatigue crack initiation using polycrystal plasticity. *Proc Roy Soc Lond A* 2004;460:1881–903.
- [31] Zhang M, Zhang J, McDowell DL. Microstructure-based crystal plasticity modeling of cyclic deformation of Ti–6Al–4V. *Int J Plast* 2007;23(8):1328–48.
- [32] Taylor GI. Plastic strain in metals. *J Inst Metals Lond* 1938;62:307–24.
- [33] Bažant ZP. Microplane model for strain-controlled inelastic behavior. In: Desai CS, Gallagher RH, editors. *London: J. Wiley*. p. 45–59 [chapter 3].
- [34] Bažant ZP, Oh BH. Microplane model for progressive fracture of concrete and rock. *J Eng Mech ASCE* 1985;111:559–82.
- [35] Caner FC, Bažant ZP. Microplane model M7 for plain concrete I: formulation. *J Eng Mech ASCE* 2013;139:1714–23.
- [36] Caner FC, Bažant ZP. Microplane model M7 for plain concrete II: calibration and verification. *J Eng Mech ASCE* 2013;139:1724–35.
- [37] Bažant ZP, Caner FC, Carol I, Adley MD, Akers SA. Microplane model M4 for concrete: I. Formulation with work-conjugate deviatoric stress. *J Eng Mech ASCE* 2000;126(9):944–53.
- [38] Bažant ZP, Bhat PD. Endochronic theory of inelasticity and failure of concrete. *J Eng Mech Div EM4* 1976:701–22.
- [39] Valanis KC. A theory of viscoplasticity without a yield surface. *Arch Mech Stossowanej* 1971;23:517–51.
- [40] Cusatis G, Pelessone D, Mencarelli A. Lattice discrete particle model (LDPM) for failure behavior of concrete I: theory. *Cem Concr Compos* 2011;33(9):881–90.
- [41] ABAQUS/explicit users manual/ABAQUS version 6.11. Dassault Systmes Simulia, Providence, RI; 2011.
- [42] Jirásek M, Bauer M. Numerical aspects of the crack band approach. *Comput Struct* 2012;110–111:60–78.
- [43] Northwestern University Information Technology. High performance computing system – quest; 2013. <<http://www.it.northwestern.edu/research/adv-research/hpc/quest/index.html>>.
- [44] Le J-L, Bažant ZP. Unified nano-mechanics based probabilistic theory of quasibrittle and brittle structures: II. Fatigue crack growth, lifetime and scaling. *J Mech Phys Solids* 2011;59:1291–321.
- [45] Bažant ZP, Qiang Yu. “Size effect testing of cohesive fracture parameters and non-uniqueness of work-of-fracture method. *ASCE J Eng Mech* 2011;137(8):580–8.
- [46] Ray S, Chandra-Kishen J. Fatigue crack growth due to overloads in plain concrete using scaling laws. *Sadhana (Indian Academy of Sciences)* 2012;37(1):107–24.
- [47] Yang JN, Liu MD. Residual strength degradation model and theory of periodic proof tests for graphite/epoxy laminates. *J Compos Mater* 1977;11:176–203.
- [48] Slowik V, Plizzari GA, Saouma VE. Fracture of concrete under variable amplitude fatigue loading. *ACI Mater J* 1996;93(3):272–83.
- [49] Zhang B, Wu K. Residual fatigue strength and stiffness of ordinary concrete under bending. *Cem Concr Res* 1997;27(1):115–26.
- [50] Award ME, Hilsdorf HK. Strength and deformation characteristics of plain concrete subjected to high repeated and sustained loads. In: Abeles symposium: fatigue of concrete, Hollywood, Fla. and Atlantic City, NJ; 1972. p. 1–13.
- [51] Cojokaru D, Karlsson AM. A simple numerical method of cycle jumps for cyclically loaded structures. *Int J Fatigue* 2006;28:1677–89.